Thermal and Structural Properties of *sn*-1,3-Dipalmitoyl-2-oleoylglycerol and *sn*-1,3-Dioleoyl-2-palmitoylglycerol Binary Mixtures Examined with Synchrotron Radiation X-Ray Diffraction

A. Minato[a,*], S. Ueno[a], J. Yano[a], K. Smith[b], H. Seto[c], Y. Amemiya[d], and K. Sato[a]

[a]Faculty of Applied Biological Science, Hiroshima University, Higashi-Hiroshima, 739, Japan, [b]Colworth Laboratory, Unilever Research, Bedford, MK44 1LQ, United Kingdom, [c]Faculty of Integrated Arts and Science, Hiroshima University, Higashi-Hiroshima, 739, Japan, and [d]Faculty of Engineering, University of Tokyo, Bunkyo-ku, Tokyo, 113, Japan

ABSTRACT: Thermodynamic and polymorphic behavior of POP (*sn*-1,3-dipalmitoyl-2-oleoylglycerol) and OPO (*sn*-1,3-dioleoyl-2-palmitoylglycerol) binary mixtures was examined using differential scanning calorimetry and conventional and synchrotron radiation X-ray diffraction. A molecular compound, β_C, was formed at the 1:1 (w/w) concentration ratio of POP and OPO, giving rise to two monotectic phases of POP/compound and compound/OPO in juxtaposition. β_C has a long-spacing value of 4.2 nm with a double chainlength structure and the melting point of 31.9°C. A structural model of the POP–OPO compound is proposed, involving the separation of palmitoyl and oleoyl chain leaflets in the double chainlength structure. In the polymorphic occurrence of the POP–OPO mixtures, the POP fraction transformed from α to β′ with no passage through γ, then transformed to β. The presence of OPO in POP promoted the β′-β transformation of POP during the melt-mediated crystallization.
JAOCS 74, 1213–1220 (1997).

KEY WORDS: Binary mixture, differential scanning calorimetry, phase behavior, polymorphism, synchrotron radiation X-ray diffraction, triacylglycerol.

Triacylglycerols (TAG) are employed in oils, margarine, cream, chocolate, and other edible fats products, and the fat structures are the major factors to determine their physical properties, such as texture, plasticity, morphology, and so on (1–4). Polymorphism is of the highest importance in the physical properties of TAG. Polymorphism of TAG has been elucidated at a molecular level for pure systems (5–7). In the practical systems, however, the fats are present in multicomponent states consisting of different types of TAG species. The first step in approaching the multicomponent systems is to study the binary systems of major TAG components, which reveal the nature of molecular interactions between the component materials at macroscopic and microscopic dimensions.

Various types of phase diagrams of the binary mixtures of TAG were reviewed by Small (8), Knoester *et al.* (9), Timms (10), and Rossell (11). As a typical mixture system, tristearin–tripalmitin (SSS–PPP) mixtures have been studied by many researchers (11–13), where metastable α and β′ forms exhibited continuous solid solutions, yet eutectic nature was revealed in the most stable β form. The formation of the molecular compound was suggested in the mixture of *sn*-1,3-dipalmitoyl-2-oleoylglycerol and *sn*-1,3-dioleoyl-2-palmitoylglycerol (POP–OPO) (P, palmitoyl; O, oleoyl) by Moran (14) who indicated two binary systems, in juxtaposition, of POP/compound and compound/OPO. In this mixture, the compound was estimated to form at an equal concentration ratio. Most recently, Engstrom (15), Koyano *et al.* (16), and Minato *et al.* (17) reported precise analyses of the mixture systems of *sn*-1,3-distearoyl-2-oleoylglycerol and 1,2-distearoyl-3-oleoylglycerol (SOS/SSO) (S, stearoyl), *sn*-1,3-distearoyl-2-oleoylglycerol and *sn*-1,3-dioleoyl-2-stearoylglycerol (SOS/OSO), and *sn*-1,3-dipalmitoyl-2-oleoylglycerol and 1,2-dipalmitoyl-3-oleoylglycerol (POP/PPO), respectively. In all the mixtures, the compound formation was observed at the 1:1 (w/w) concentration ratio, indicating specific molecular interactions through the acyl chain moieties. It is worth noting that oleoyl chains are commonly present in all the component TAG of the mixture systems as saturated–oleoyl mixed acid TAG (15–17).

From a technological implication, the occurrence of crystallization and transformation of TAG in the metastable forms is the important process leading to the growth of hard and brittle crystals. Therefore, it is interesting to elucidate the molecular structures and kinetic properties of the mixture systems. Recent studies showed that the effect of the *trans* configuration of the double bond is to modify the phase behavior through partial solubilization in the mixtures of trielaidin and triolein (EEE–OOO) and EEE–SSS (E, elaidoyl) (18).

The use of a time-resolved synchrotron radiation X-ray diffraction (SR–XRD) must be helpful for the understanding of the dynamic phenomena of the phase and structural behavior of the mixture systems. Recent SR–XRD studies on the mixtures of PPP–SSS (19–21), PPP–POP (17), and POP–PPO (22) have revealed the dynamic aspects of the polymorphic transformations in complicated mixture phases.

*To whom correspondence should be addressed.

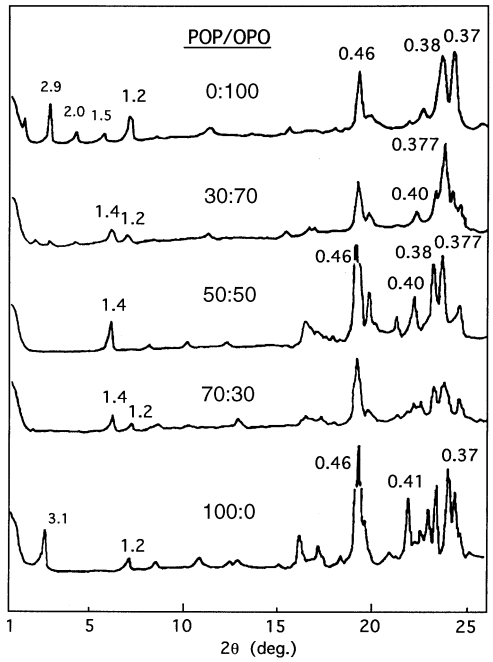

FIG. 1. X-ray diffraction (XRD) spectra of the most stable forms of *sn*-1,3-dipalmitoyl-2-oleoylglycerol and *sn*-1,3-dioleoyl-2-palmitoylglycerol (POP/OPO) binary mixtures at different concentrations, taken at 15°C.

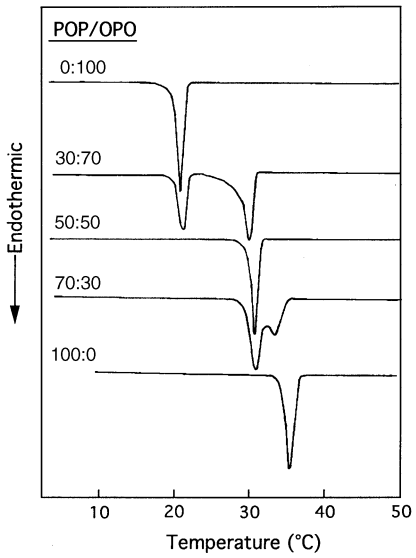

FIG. 2. Differential scanning calorimetry (DSC) heating thermograms of POP/OPO binary mixtures in the most stable polymorphs. See Figure 1 for other abbreviation.

In the present work, the dynamical properties of polymorphic behavior of the OPO–POP binary mixtures forming the molecular compound were studied using differential scanning calorimetry (DSC) and XRD with conventional and synchrotron radiation. The polymorphic behavior of POP has fully been reported, exhibiting conversions in the chainlength structure of double–triple–double–triple (23). However, the polymorphic behavior of OPO has not been reported except for the most stable β form (14). Therefore, the polymorphism of OPO also will be reported here.

It is worthy to note that the mixture systems of POP and OPO may have an industrial implication of blending of vegetable oils using palm oil through interesterification or mixing. The winterizing process often causes the formation of sediments. The sediments involving POP and OPO are major components, possibly forming the mixture compounds.

EXPERIMENTAL PROCEDURES

Materials. POP was provided by Unilever Research Laboratory (Colworth, United Kingdom), and OPO was purchased from Sigma Chemical Co. (St. Louis, MO) with purity higher than 99%. Both samples were employed without further purification. The binary mixtures of POP and OPO were melted at 50°C and mixed using a vortex mixer. Thermodynamic equilibration to obtain the most stable forms was done by incubating at 15°C below POP 50% concentration and at 29°C above POP 50% concentration over 1 mon. The occurrence and transformation of the metastable forms were induced by the thermal treatments described in the next section.

Methods. Thermal measurements were performed with DSC-8230 (Rigaku, Tokyo, Japan) at rates of 5 and 15°C/min for cooling, and of 5°C/min for heating. The crystal forms were assessed by powder XRD (Rigaku Geigerflex, λ = 0.1542 nm; Tokyo, Japan). SR–XRD (λ = 0.15 nm) was taken at the Photon Factory (PF) in the National Laboratory for High-Energy Physics (Tsukuba, Japan). The XRD spectra were recorded 10 s with two gas-filled one-dimensional position-sensitive (PSPC) detectors. One was for the small-angle region (Rigaku; 512 channels over a total length of 200 mm), and the other was for the wide-angle region (MAC Science, Tokyo, Japan; 512 channels over a total length of 50 mm). The distance between the sample and PSPC was 1110 mm (small-angle) and 280 mm (wide-angle). The temperature of the sample was controlled by Mettler DSC-FP84 (Mettler Instrument Corp., Greifensee, Switzerland) with FP99 system software. The sample cell with diamond windows of 1-mm thickness was employed, and the thickness of the sample was 2 mm. The thermal conditioning was the same as in the case of DSC measurements.

RESULTS AND DISCUSSION

Table 1 summarizes the structural and thermal data of four forms of OPO; α, β′, β_2, and β_1. The details of the experimental evidences of the XRD and DSC will be shown later, together with those of the mixtures with POP.

(i) Phase diagram. Figure 1 shows the XRD patterns of the most stable forms of the POP/OPO binary mixtures, which were obtained by incubating the mixtures at 29°C over 7 d for the samples of the POP concentration above 50%, and at 20°C over 7 d for the POP concentrations below 50%.

As for long-spacing values, pure POP and OPO showed

TABLE 1
Melting Points and X-Ray Diffraction Long Spacing of *sn*-1,3-Dioleoyl-2-palmitoylglycerol

	α	β′	β_2	β_1
Melting point (°C)	−18.3	11.7	15.8	21.9
Long spacing (nm)	4.8	4.4	5.6	6.4
Chainlength structure	Double	Double	—	Triple

6.2 and 6.0 nm, respectively, both of which correspond to β forms of the triple chainlength structure. By mixing the two samples, a new long-spacing peak appeared at 1.4 nm, corresponding to (003) reflection of 4.2 nm. The strength of this spectrum increased on approaching the 50:50 ratio from both sides of the pure POP and OPO. The single peak of 4.2 nm was obtained at the POP/OPO = 50:50 concentration.

As for the short-spacing spectra, a strong peak at 0.46 nm was observed in all the mixtures. This spectrum is characteristic of triclinic parallel ($T_{//}$) subcell structure (5). The pure POP showed a typical short-spacing pattern of β_1 form (23), and the spectrum of the pure OPO is specific of β_1 form. At the 50:50 (1:1, w/w) ratio, however, a unique short-spacing pattern was obtained, definitely differing from those of β forms of POP and OPO. Above the POP 50% concentration, the superposition of the spectra of the 50:50 (1:1, w/w) mixture and POP β_2 were obtained. Similarly, short-spacing patterns were equivalent to the superposition of the spectra of the 50:50 (1:1, w/w) mixture and OPO β_1 below the POP 50% concentration. These properties are quite similar to those of the SOS/OSO mixture system (16).

The DSC heating thermograms of the most stable polymorphs of the mixed and pure systems are shown in Figure 2. The single endothermic peaks were observed at 36.5 and 21.9°C at the POP 100 and 0% concentrations, respectively. At the equal ratio of POP and OPO, the single endothermic peak was also observed at 31.9°C, whereas two endothermic peaks appeared at the other concentrations. Below the POP 50% concentration, the higher melting points increased with increasing POP contents. By contrast, no change of the lower

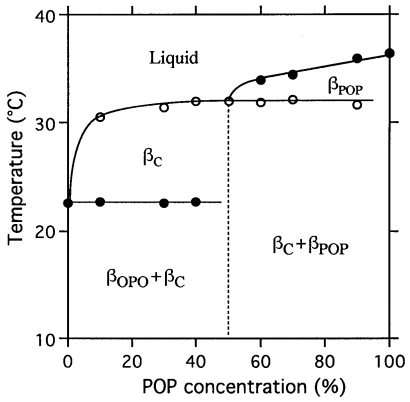

FIG. 3. The melting behavior of POP/OPO binary mixtures in the most stable form. See Figure 1 for abbreviation.

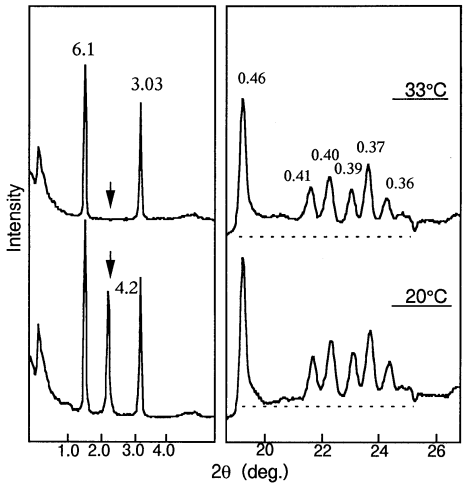

FIG. 4. Temperature dependence of XRD spectra of the most stable form of the POP/OPO = 90:10 mixture (unit:nm). See Figure 1 for abbreviations.

melting points around 31.9°C was observed. Above the POP 50% concentration, the higher melting points increased with increasing POP contents from 31.9 to 36.5°C, and the lower melting points did not change around 31.9°C.

Figure 3 shows the phase diagram of POP/OPO binary mixture system constructed from the melting points shown in Figure 2, which exhibits two monotectic regions divided at the POP 50% concentration. Figure 4 shows the XRD spectra of the POP/OPO mixtures of 90:10 in the most stable polymorph taken at 20 and 33°C. The low-angle XRD pattern at 20°C was the same as that of the POP/OPO = 70:30 mixture (Fig. 1). However, the (001) reflection of 4.2 nm disappeared by raising the temperature to 33°C, where the spectra of (001) and (002) of POP β_2 were still present. This clearly demonstrates the monotectic nature of the mixtures of POP (β)/compound (β_C) and compound (β_C)/OPO (β) in the most stable polymorph, as shown in Figure 3. This result is consistent with the phase diagram reported by Moran (14) except for the details of the crystalline structures.

(ii) Kinetic phase properties. Figure 5 shows DSC cooling thermograms obtained by quenching the mixture liquid from 50 to −30°C at a rate of 15°C/min for obtaining metastable polymorphs. Upon cooling, POP and OPO crystallized at −21.3 and 11.0°C, respectively. At the POP 30% concentration, two exothermic peaks were observed at −6.9 and −21.7°C, corresponding to the crystallization of OPO α and the compound α (α_C), respectively. At the POP 70% concentration, two exothermic peaks of 2.7 and 7.0°C were obtained. The two peaks correspond to the crystallization of α_C and POP α, which were confirmed by the wide-angle XRD spectra. At the POP/OPO = 50:50 concentration, two exothermic peaks were observed at 3.6 and 0.7°C, both of which were due to α as confirmed by the wide-angle XRD spectra. Figure 6 displays the crystallization temperatures of the POP/OPO mixtures obtained by the rapid cooling shown in Figure 5. This kinetic phase diagram exhibits two monotectic phases,

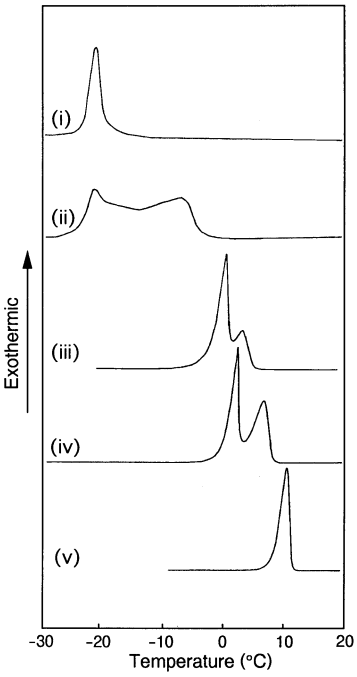

FIG. 5. DSC cooling thermograms of POP/OPO mixtures at a rate of 15°C/min. POP/OPO = (i) 0:100, (ii) 30:70, (iii) 50:50, (iv) 70:30, and (v) 100:0. See Figures 1 and 2 for abbreviations.

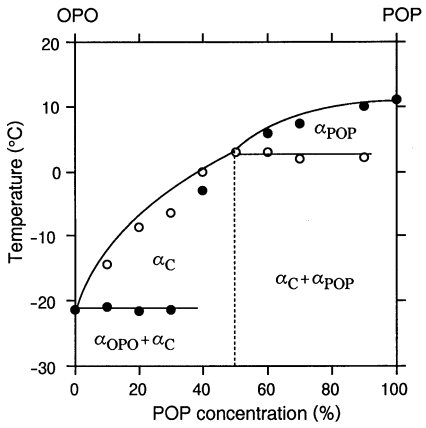

FIG. 6. Crystallization temperatures of POP/OPO mixtures at a cooling rate of 15°C/min. ●, for α_{OPO} and α_{POP}; ○, for α_C. See Figure 1 for abbreviation.

which are similar to the phase diagram of POP/OPO mixture in the most stable state (Fig. 3). It was found that the compounds POP and OPO are not miscible in the α form.

DSC heating (5°C/min) thermograms of the samples, obtained by the quenching shown in Figure 5, are shown in Figure 7. As for the pure OPO, the heating thermogram showed a small endothermic peak at −18.0°C, which was soon followed by an exothermic peak at −16°C. These two peaks correspond to the melting of the less stable form and rapid crystallization of the more stable form. In the wide-angle XRD spectra of the pure OPO, the single spectrum specific to α at 2θ = 21° (0.42 nm) was observed at −30°C, and β′ form and β_1 form were observed at −15 and at 10°C, respectively. This polymorphic behavior of OPO is similar to that of OSO (24).

At the POP 30% concentration, the compound melted at 32°C, and the occurrence behavior of OPO in this mixture was similar to that of the pure OPO, in which $\alpha \rightarrow \beta' \rightarrow \beta_1$ transformation occurred. At the POP 50% concentration, α_C transformed to β_C at 16°C, then melted at 31.9°C. The polymorphic forms of α_C and β_C were confirmed by the XRD measurements. Above the POP 50% concentration, the same results were obtained between the crystallization by rapid- and slow-cooling process.

From here, precise analyses of the transformation behavior of the POP/OPO mixtures with DSC and SR–XRD during the heating process will be described. In particular, a time-resolved SR–XRD experiment enabled structural analyses of the polymorphic transformations occurring during the DSC thermal treatments.

Figure 8 shows DSC and SR–XRD data of metastable forms of the POP/OPO = 10:90 mixture, which was quenched from 40 to −30°C, incubated for 5 min at −30°C, then heated to 40°C at a rate of 5°C/min. A small endothermic peak appeared at −2°C, which was followed by an exothermic peak at 6°C, and three large endothermic peaks appeared at 16.3, 20.7, and 28.7°C, as shown in Figure 8A. This melting pattern was the superposition of polymorphic transformations in OPO fractions and the POP/OPO compound fractions.

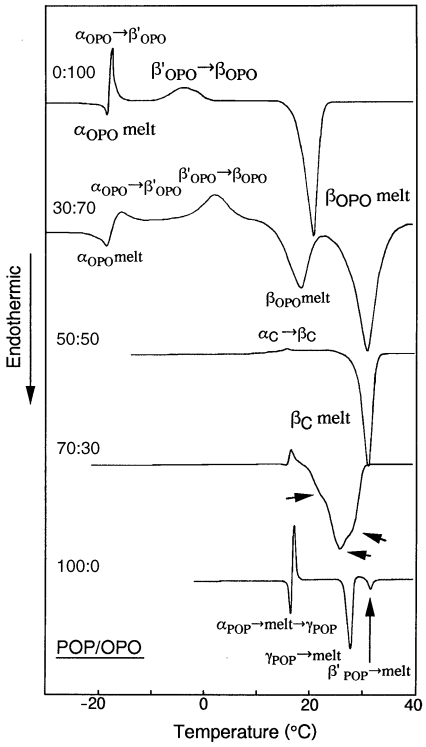

FIG. 7. DSC heating thermograms of the mixtures at different concentrations of POP/OPO after quenching at a rate of 15°C/min exhibited in Figure 5. See Figures 1 and 2 for abbreviations.

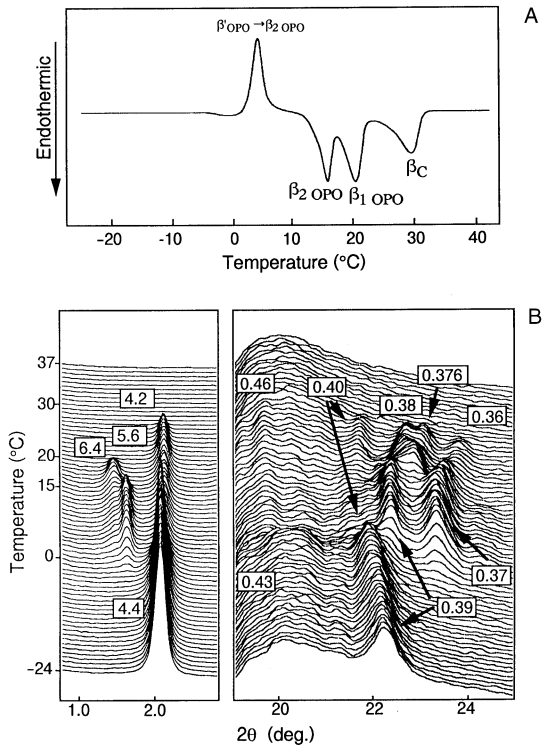

FIG. 8. (A) DSC heating thermogram and (B) synchrotron radiation XRD spectra of metastable forms of POP/OPO = 10:90 mixture (unit:nm). See Figures 1 and 2 for abbreviations.

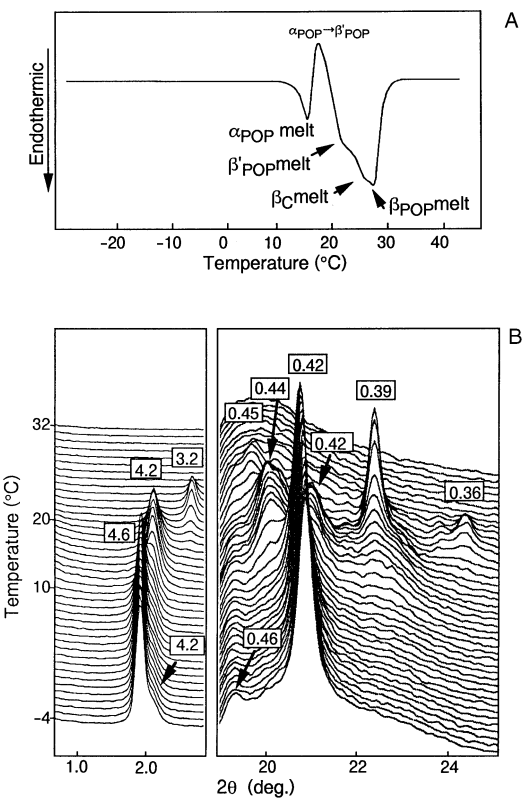

FIG. 9. (A) DSC heating thermogram and (B) synchrotron radiation XRD spectra of metastable forms of POP/OPO = 90:10 mixture (unit:nm). See Figures 1 and 2 for abbreviations.

The polymorphic occurrence and transformation of the molecular compound and OPO were revealed by the low- and wide-angle SR–XRD spectra, taken under the same temperature variation as that of DSC, as shown in Figure 8B. In the small-angle region, the broad peak at 4.4 nm appeared during the incubation at −30°C. Then, on heating, a new spectrum of 5.6 nm appeared around −5°C. The peak intensity of 4.4 nm was decreased during this heating process, and gradually converted to 4.2 nm around 0°C. At 16°C, the peak of 5.6 nm disappeared; instead, a peak at 6.4 nm appeared, yet 4.2 nm was still present. Correspondingly, two short-spacing spectra of 0.43 and 0.40 nm and a small spectrum at 0.42 nm were observed after the incubation at −30°C. Each spectrum corresponds to β′ and α, indicating that β'_{OPO} and α_C have the long-spacing value of 4.4 nm with the double chainlength structure. Upon heating, the short-spacing spectra changed to three spectra (0.46, 0.39, and 0.37 nm) around −5°C. Then, the spectra characteristic of β appeared at 16°C. Since the peaks at 5.6 and 6.4 nm were observed in the pure OPO, the occurrence and disappearance of the long-spacing spectra of the 5.6 and 6.4 nm in Figure 8 mean the transient occurrence and melting of β_2 and β_1 of the OPO fractions, both of which are triple chainlength. The final form of β_C of the POP/OPO compound has a long-spacing value of 4.2 nm with the double chainlength structure.

Figure 9 shows the DSC heating thermogram and SR–XRD data of the metastable forms of the POP/OPO = 90:10 mixture. The heating thermogram (Fig. 9A) showed an endothermic peak at 16.3°C, which was soon followed by an exothermic peak at around 17.5°C. These two peaks correspond to the melting of the less stable forms and rapid crystallization of the more stable forms. Further heating showed three melting peaks at 22, 25, and 27°C, which correspond to three endothermic peaks of the POP/OPO = 70:30 mixture shown in Figure 7 (arrows).

The SR–XRD spectra (Fig. 9B) exhibited the following transformations. Soon after the incubation at −20°C, a strong peak of 4.6 nm and a shoulder peak of 4.2 nm were present. Upon heating, the peak of 4.6 nm disappeared at 16°C, and the intensity of 4.2 nm peak gradually increased. Then the peak at 4.2 nm disappeared at 22°C, and a new spectra of 3.2 nm appeared at 18°C, and disappeared at 26°C. Correspondingly, the short-spacing XRD revealed the peaks at 0.42 and 0.46 nm, just after the incubation at −20°C, indicating the coexistence of α and β forms. Upon heating, two spectra at 0.44 and 0.39 nm, corresponding to β′ form, appeared at the expense of the peaks of 0.46 and 0.43 nm. Further heating raised the peak at 0.45 nm characteristic of β after the melting of β′ at 22°C. The form finally obtained was β_{POP}, because the corresponding small-angle SR–XRD peak of 3.2 nm was the (002) reflection of β of triple chainlength. The data of DSC and SR–XRD in Figure 9 indicate the independent transformations of the POP and compound fractions in the POP/OPO = 90:10 mixture.

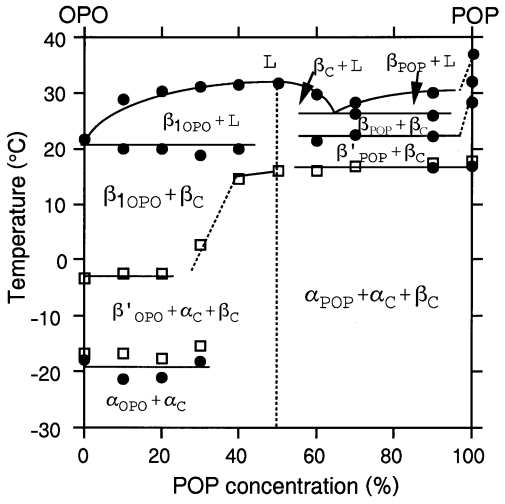

FIG. 10. Kinetic phase diagram constructed by DSC heating thermograms after quenching at a rate of 15°C/min; ●, endothermic; □, exothermic; L, liquid. See Figures 1 and 2 for abbreviations.

Figures 10 and 11 compare kinetic phase diagrams obtained by the DSC heating thermograms, combined with the SR–XRD data, of the metastable forms taken for the two mixture samples obtained after the quenching at a rate of 15°C/min (Fig. 10) and 5°C/min (Fig. 11). The polymorphic behavior of the two mixture samples was the same in the concentration ranges above POP 50%. However, below the POP 50% concentrations, the polymorphic behavior of the OPO fraction was different in the two mixture samples. The mixtures formed by the quenching at the rate of 5°C/min exhibited β′, β_2, and β_1 forms of the OPO fraction. By contrast, in the mixtures formed by the 15°C/min quenching (Fig. 11), α_{OPO} was formed and the temperature range of the occurrence

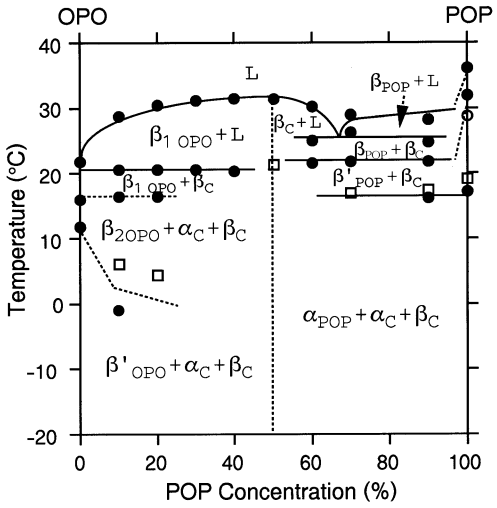

FIG. 11. Kinetic phase diagram constructed by DSC heating thermograms after quenching at a rate of 15°C/min; ●, endothermic; □, exothermic; L, liquid. See Figures 1 and 2 for abbreviations.

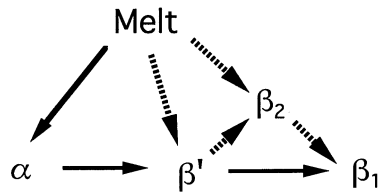

FIG. 12. Polymorphic transitions of OPO. See Figure 1 for abbreviation.

of β′ was raised compared to those shown in Figure 10. In addition, the differentiation of two β forms of OPO was hindered.

These results indicate that the polymorphic occurrence of the OPO fractions is sensitive to the rate of quenching, as shown in Figure 12.

Concerning the structure model of the POP–OPO compound (Fig. 13), Table 2 summarizes the thermal and structural data of the polymorphic forms of the molecular compounds of POP–OPO, POP–PPO (17), SOS–OSO (16), and SOS–SSO (15). Long- and short-spacing XRD and DSC entropy of fusion are available to discuss the structure model of β_C of the POP–OPO compound. The XRD measurements showed that β_C revealed the subcell structure of $T_{//}$, having the double chainlength structure. The oleoyl and palmitoyl chains must be packed in each leaflet of the double chainlength lamellae as shown in Figure 12 like the SOS–OSO compound (16).

The ordering state in the crystal phase can be discussed on the basis of the entropy of fusion, ΔS, which is 0.42 kJ/mol · deg for β_C of POP–OPO (Table 2). This value is similar to those of POP β_1 (0.42 kJ/mol · deg) (23) and SOS–OSO β (0.44 kJ/mol · deg). It is assumed that compact packing of oleoyl and palmitoyl chains in the same leaflet in β_C may arouse serious steric hindrance, because of the bent geometrical structure of oleoyl chains. Consequently, the structure model of POP–OPO compound in Figure 13 is most plausible.

The detailed molecular structures are open to future studies. It is quite interesting to elucidate precise subcell packing and conformation, configuration of olefinic group, glycerol structures, and methyl end packing. With regard to the con-

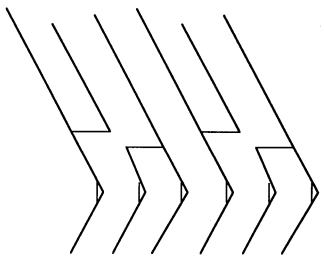

FIG. 13. Structure model of the POP–OPO compound. See Figure 1 for abbreviation.

TABLE 2
Thermal and Structural Properties of Polymorphic Forms of POP–PPO, POP–OPO, SOS–SSO, and SOS–OSO Compounds[a]

	POP–OPO		POP–PPO[b]			SOS–SSO[c]		SOS–OSO[d]
	α	β	α	β′	β	α	β	β
T_m (°C)	n.a.	32.0	15.2	27.2	31.2	26	40.6	36
ΔH_f (kJ/mol)	n.a.	130	n.a.	90	97	n.a.	124	135.3
ΔS_f (kJ/mol • deg)	n.a.	0.42	n.a.	0.30	0.32	n.a.	0.39	0.44
L.S. (nm)	4.7	4.24	4.6	4.2	4.1	8.3	4.5	4.5
Chainlength structure	Double	Double	Double	Double	Double	Double	Double	Double

[a]T_m, melting point; ΔH_f, enthalpy of fusion; ΔS_f, entropy of fusion; L.S., long spacing; n.a., not available. POP–OPO, *sn*-1,3-dipalmitoyl-2-oleoylglycerol–*sn*-1,3-dioleoyl-2-palmitoylglycerol; P, palmitoyl; O, oleoyl.
[b]Reference 17.
[c]Reference 15.
[d]Reference 16.

figuration of the olefinic group, it is notable to remember that the diversity of molecular structures of *cis*-unsaturated fatty acids has been revealed in oleic acid (25), erucic acid (26), and petroselinic acid (27). The diversity may be seen in the subcell structures of saturated–oleoyl mixed-acid TAG in pure systems and their mixtures systems. For this purpose, the analysis using multitechniques such as Fourier transform infrared spectroscopy will be quite useful, and work on this line is in progress.

To summarize, the following phase behavior of POP–OPO binary mixtures was observed. (i) The POP–OPO binary mixtures formed the molecular compound at the 1:1 concentration ratio in the most and metastable forms. (ii) The stable phase diagram and kinetic phase diagrams of the POP–OPO mixtures exhibited two monotectic phases of OPO/compound and compound/POP in a juxtapositional way. (iii) The POP fraction transformed from α to β′, then transformed to β. The presence of OPO in POP promoted the β′-β transformation of POP during the melt-mediated crystallization.

REFERENCES

1. Formo, M.W., in *Bailey's Industrial Oil and Fat Products*, Vol. 1, edited by D. Swern, John Wiley & Sons, New York, 1979, pp. 177–232.
2. deMan, J.M., in *Fatty Acids in Food and Their Health Implications*, edited by C.K. Chow, Marcel Dekker, New York, 1992, pp. 17–45.
3. Timms, R.E., in *Fats in Food Products,* edited by D.P.J. Moran and K.K. Rajah, Blackie Academic & Professional, London, 1994, pp. 1–24.
4. Sato, K., in *Advances in Applied Lipid Research*, edited by F. Padley, JAI Press, New York, 1996, Vol. 2, pp. 213–268.
5. Hagemann, J.W., in *Crystallization and Polymorphism of Fats and Fatty Acids*, edited by N. Garti and K. Sato, Marcel Dekker, New York, 1988, pp. 9–95.
6. Yano, J., S. Ueno, K. Sato, T. Arishima, N. Sagi, F. Kaneko, and M. Kobayashi, FT–IR Study of Polymorphic Transformations in SOS, POP and POS, *J. Phys. Chem. 97*:12967–12973 (1993).
7. Arishima, T., K. Sugimoto, R. Kiwata, H. Mori, and K. Sato, ^{13}C Cross-Polarization and Magic-Angle Spinning Nuclear Magnetic Resonance of Polymorphic Forms of Three Triacylglycerols, *J. Am .Oil Chem. Soc. 73*:1231–1236 (1996).
8. Small, D.M., in *The Physical Chemistry of Lipids*, Plenum, New York, 1986, pp. 345–395.
9. Knoester, M., P. De Bruijne, and M. Van Den Tempel, The Solid–Liquid Equilibrium of Binary Mixtures of Triglycerides with Palmitic and Stearic Chains, *Chem. Phys. Lipids 9*:309–319 (1972).
10. Timms, R.E., Phase Behavior of Fats and Their Mixtures, *Prog. Lipid Res. 23*:1–38 (1984).
11. Rossell, J.B., Phase Diagrams of Triglyceride Systems, *Adv. Lipid Res. 5*:353–408 (1967).
12. Lutton, E.S., Phase Behavior of Triglyceride Mixture Involving Primarily Tristearin, 2-Oleyldistearin, and Triolein, *J. Am. Oil Chem. Soc. 32*:49–53 (1955).
13. Kerridge, R., Melting-Point Diagrams for Binary Triglyceride System, *J. Chem. Soc.*:4577–4579 (1952).
14. Moran, D.P.J., Phase Behavior of Some Palmito-Oleo Triglyceride Systems, *J. Appl. Chem. 13*:91–100 (1963).
15. Engstrom, L., Triglyceride Systems Forming Molecular Compounds, *J. Fat Sci. Technol. 94*:173–181 (1992).
16. Koyano, T., I. Hachiya, and K. Sato, Phase Behavior of Mixed Systems of SOS and OSO, *J. Phys. Chem. 96*:10514–10520 (1992).
17. Minato, A., S. Ueno, J. Yano, Z.H. Wang, H. Seto, Y. Amemiya, and K. Sato, Synchrotron Radiation X-Ray Diffraction Study on Phase Behavior of PPP–POP Binary Mixtures, *J. Am. Oil Chem. Soc. 73*:1567–1572 (1996).
18. Desmedt, A., C. Culot, C. Deroanne, F. Durant, and V. Gibon, Influence of *cis* and *trans* Double Bonds on the Thermal and Structural Properties of Monoacid Triglycerides, *Ibid. 67*:653–660 (1990).
19. Kellens, M., W. Meeussen, C. Riekel, and H. Reynaers, Time-Resolved X-Ray Diffraction Studies of the Polymorphic Behavior of Tripalmitin Using Synchrotron Radiation, *Chem. Phys. Lipids 52*:79–98 (1990).
20. Kellens, M., W. Meeussen, and R. Gehrke, Synchrotron Radiation Investigations of the Polymorphic Transitions of Saturated Monoacid Triglycerides. Part 1: Tripalmitin and Tristearin, *Ibid. 58*:131–144 (1991).
21. Kellens, M., W. Meeussen, A. Hammersley, and H. Reynaers, Synchrotron Radiation Investigations of the Polymorphic Transitions of Saturated Monoacid Triglycerides. Part 2: Polymorphism Study of a 50:50 Mixture of Tripalmitin and Tristearin During Crystallization and Melting, *Ibid. 58*:145–158 (1991).
22. Minato, A., S. Ueno, K. Smith, Y. Amemiya, and K. Sato, Thermodynamic and Kinetic Study on Phase Behavior of Binary Mixtures of POP and PPO Forming Molecular Compound Systems, *J. Phys. Chem.*, in press.
23. Sato, K., T. Arishima, Z.H. Wang, K. Ojima, N. Sagi, and H.

Mori, Polymorphism of POP and SOS. I. Occurrence and Polymorphic Transformation, *J. Am. Oil Chem. Soc. 66*:664–674 (1989).
24. Kodali, D.R., D. Atkinson, T.G. Redgrave, and D.M. Small, Structure and Polymorphism of 18-Carbon Fatty Acyl Triglycerols: Effect of Unsaturation and Substitution in the 2-Position, *J. Lipid Res. 28*:403–413 (1987).
25. Kobayashi, M., F. Kaneko, K. Sato, and M. Suzuki, Vibrational Spectroscopic Study on Polymorphism and Order-Disorder Phase Transition in Oleic Acid, *J. Phys. Chem. 90*:6371–6378 (1986).
26. Kaneko, F., M. Kobayashi, Y. Kitagawa, Y. Matsuura, K. Sato, and M. Suzuki, Structure of the γ Phase of Erucic Acid, *Acta Crystallogr. C48*:1060–1063 (1992).
27. Kaneko, F., M. Kobayashi, Y. Kitagawa, Y. Matsuura, K. Sato, and M. Suzuki, Structure of the Low-Melting Phase of Petroselinic Acid, *Ibid. C48*:1054–1057 (1992).

[Received February 25, 1997; accepted June 1, 1997]